Journal of Intelligent Material Systems and Structures
XX(X):1–20

DOI: 10.1177/ToBeAssigned
www.sagepub.com/
SAGE

Delamination of surface accretions with structural waves: piezo-actuation and power requirements

Michał K. Kalkowski[1], Timothy P. Waters[1] and Emiliano Rustighi[1]

Abstract

Unwanted accretions on structures, such as aircraft and wind turbine icing or deposits in pipes, are a common problem, which can pose a serious safety threat if not treated effectively and punctually. In this paper we investigate the capability of piezo-excited structural waves for delaminating accreted material. The core of the concept is to utilise the stress distribution associated with waves propagating through the structure to detach unwanted build-up. We apply a wave-based technique for modelling piezoelectric excitation based on semi-analytical finite elements to calculate the shear stress at the interface between the host structure and the accretion generated by piezo-actuated waves. Our analyses include the effects of the actuator's dynamics and allow for comparing different types of actuators, identifying the most effective frequency of excitation and formulating realistic power requirements. For the dual purpose of proof of concept and validation of the model, we present a demonstration experiment in which patches of accreted material are removed from a beam-like waveguide with emulated anechoic terminations using ultrasonic excitation.

Keywords

accretion removal, ultrasonic de-icing, smart structures, structural waves, delamination, piezoelectric actuators

Introduction

Motivation

An unwanted material built-up on various types of structures is a common engineering problem which seriously affects performance and safety of operation. For aircraft, ice accumulation during flight seriously deteriorates the aerodynamic properties of the wing profile. Among other components, it also affects engine nacelles disturbing the flow and possibly leading to ice ingestion. A similar phenomenon causes wind turbines to experience a drop in efficiency and potentially severe injury or damage to nearby objects due to self-induced ice shedding. Pipelines often suffer from deposits on their internal walls which degrade flow parameters and influence the quality of a transported medium.

From the aforementioned examples, aircraft icing receives the greatest attention from engineers and researchers. The literature offers a multitude of contributions regarding the physics of ice accretion and methods of tackling icing. However, the increased use of composites in modern aircraft has introduced new complications for incorporating standard (especially thermal) methods. Their drawbacks and limitations are still a challenge to overcome and an inspiration for research in the area.

---

[1] University of Southampton, UK

Corresponding author:
Michał K. Kalkowski, Institute of Sound and Vibration Research, University of Southampton, Highfield, Southampton SO17 1BJ, UK

Email: M.Kalkowski@soton.ac.uk

A potentially promising alternative to the traditional methods for tackling the build-up of accretions is a mechanical approach in which the accreted layer is removed with the aid of structural waves induced by piezoelectric actuators.

State of the art

The idea of tackling the problem of ice accretion by means of ultrasonic waves was first proposed by Adachi et al. (1998), who noticed that ultrasonic vibration reduces the frost accumulation on a thin metallic plate. The possibility of using guided waves for de-icing has since been developed at Pennsylvania State University. The PhD thesis of Ramanathan (2005) investigated the application of shear horizontal waves as a way of provoking delamination in an iced aluminium plate. Although delamination was observed during the experiments, thermal processes seem to have played a crucial role in achieving this effect. In parallel, Seppings (2005) employed ultrasonic vibration for removing ice and frozen sucrose build-up from pipes.

Palacios implemented a 3D finite element model for the preliminary design of a de-icing system and provided impedance matching for excitation, which lead to very promising experimental results (Palacios 2006, 2008; Palacios et al. 2011a,b). Instantaneous delamination was observed for both freezer and impact ice, proving the feasibility of the method. Palacios' extensive experimental work compared various actuator designs and discussed a series of problems associated with ultrasonic de-icing. The follow-up study by Overmeyer et al. (2011) addressed design issues such as the actuators' optimal bonding conditions and techniques to avoid actuator cracking. An experimental demonstration on a helicopter blade with a few actuators attached was also presented. One possible way of optimising structural design for ultrasonic de-icing purposes was proposed by Zhu (2010). The generated stress was enhanced by introducing patterned inclusions to the structure resulting in a series of local stress concentration points. Further developments include a recent work by DiPlacido et al. (2013) showing that the transient effects associated with switching piezoelectric actuation provide much higher stress than the steady-state response. The enhancement of the area coverage of ultrasonic de-icing by phasing an array of actuators has been considered by Borigo (2014).

A few researchers focused on predominantly experimental investigation into the effect of ultrasonic vibration on ice (Li and Chen 2014; Tan et al. 2015). A new type of a piezoelectric transducer was considered by Wang et al. (2015). Finally, a more complex material modelling including cohesive material theory and mixed-mode fracture energy approach was employed by Młyniec et al. (2014).

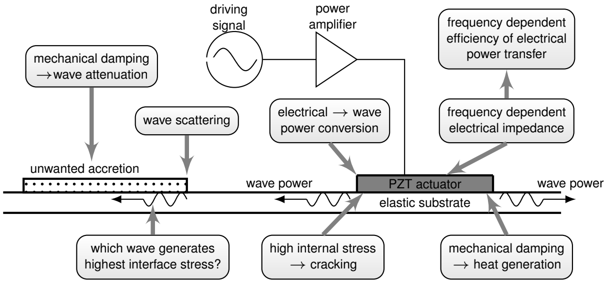

Figure 1. Key aspects of removing surface accretions with piezo-actuated structural waves

The challenges encountered during practical implementation of the aforementioned concepts can be summarised in a list of critical issues pictured schematically in Figure 1:

- effective driving of the actuator; impedance matching between the driving source and the actuator is essential.
- actuator temperature which elevates at resonance due to mechanical damping; this is undesirable, since the expected effect of ultrasonic action should be achieved instantaneously and by low power mechanical means but also because the actuator's properties change with temperature.
- cracking or self-debonding of the actuator driven with high electric field.
- electrical-to-mechanical wave power conversion efficiency and its influencing factors.
- interface stress generation efficiency of particular waves (informing actuation design).
- wave attenuation; waves that propagate energy along the accretion are not desirable.

Aims of the paper

The results presented in the literature to date are promising, but there are still many aspects to be developed and investigated. Most of the references recalled above are supported with finite element models representing ultrasonic vibration. Consequently, factors of secondary interest such as the dimensions of the plate and the boundary conditions play a key role. Although the aforementioned authors refer to wave models to calculate stress distributions under free wave propagation, they resort to FE models to predict piezo-actuated response. The nature of the interaction of structural waves with unwanted accretions is still not clear and the influence of the boundary conditions cannot be separated from the results. Moreover, electrical power requirements for accretion removal with incident waves have not been reported to our best knowledge.

In this paper we propose a wave-based approach to both modelling and experiments which attempts to provide a deeper understanding of the conditions facilitating delamination and bridge the gap between free wave theory and finite element models. A realistic model of piezoelectric excitation in the wave domain allows for including the dynamics of the actuator and assessing its effect on the generated stress. Moreover, insight into wave composition of the response is retained. The key aims of this work include determining realistic electrical power requirements for delaminating accretions with incident waves and providing an experimental validation of the proposed modelling approach for stress prediction.

Outline of the paper

The paper is outlined as follows. We start from the free wave perspective by discussing the origin of high interface stress and the profound effect of wave attenuation. The actuation mechanism is introduced next using a wave-based model developed in our previous work (Kalkowski et al. 2016). The model is then employed for simulating interface shear stress generated by two types of piezoelectric actuators for two illustrative structures. The results support a discussion on the efficiency of particular waves and power requirements for de-icing. The final part of the paper reports an experiment on delaminating an accretion from a waveguide with emulated anechoic terminations.

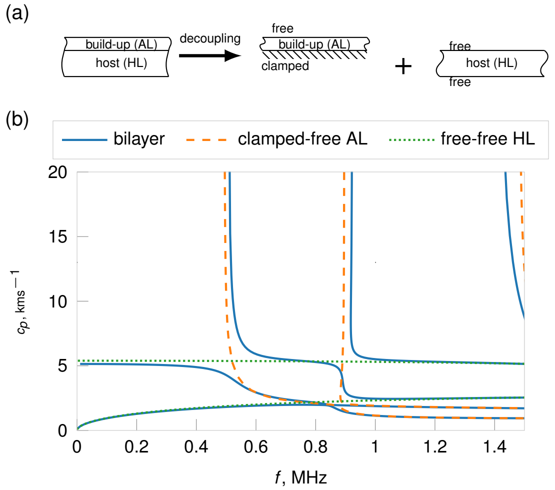

Figure 2. Decoupling of waves in an elastic bilayer: (a) schematic respresentation; (b) dispersion curves in an elastic bilayer (solid line) together with the host layer (HL) asymptote (dotted line) and the accreted layer (AL) asymptote (dashed line).

Free wave perspective

A free wave perspective allows us to identify those waves which seem to be particularly effective in generating high interface shear stress. The discussion refers to waves in plates in plane strain which are classified as either of two main types – Lamb waves and shear horizontal (SH) waves (for isotropic materials). Similar investigations have been carried out by some of the aforementioned authors (Palacios and Smith 2008; Zhu 2010). The following paragraphs aim to provide further physical explanation and a link to subsequent analyses.

For most practical cases (including ice accretion) the bond created by the build-up is weaker in shear than in tension (Chu and Scavuzzo 1991), hence the attention is focused on the interface shear stress hereafter. From the three shear stress components, the transverse shear stresses are expected to contribute to inducing delamination (Voyiadjis and Woelke, P. 2008). Given that z is chosen as a propagation direction and y as the thickness direction in this paper, σ_{yz} and σ_{yx} are the components of interest. Under

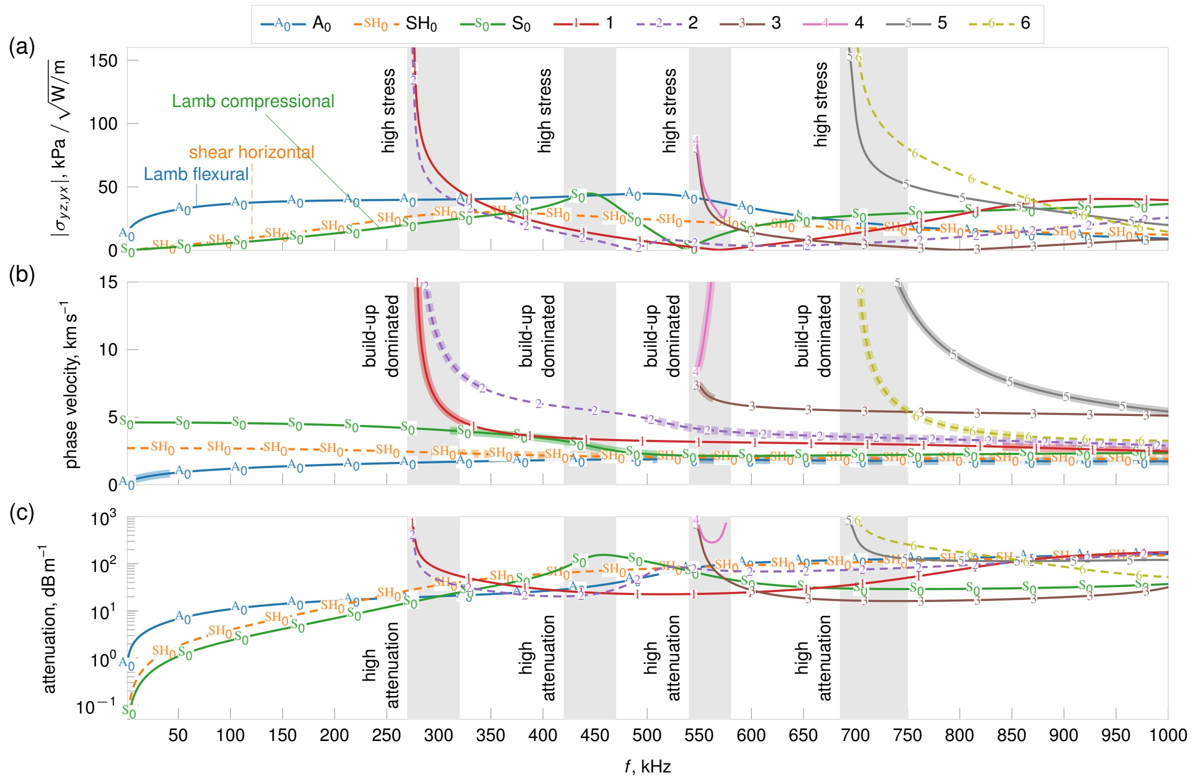

Figure 3. The relationship between the interface stress, wave attenuation, and energy distribution for a 1 mm thick aluminium plate in plane strain covered with a 2 mm glaze ice accretion; highlighted frequency regions correspond to local interface stress peaks: (a) power-normalised interface shear stress; (b) dispersion curves - thick lines indicate that the majority of wave energy ($> 60\%$) propagates along the accretion; (c) attenuation curves.

the plane strain assumption σ_{yz} is non-zero for Lamb-type waves, whereas σ_{yx} is non-zero for SH waves.

Accretions are usually of a much lower stiffness than the host waveguide. Therefore, waves propagating in a structure covered with accretion demonstrate characteristics typical for weakly coupled systems (e.g. elastic bilayers), schematically presented in Figure 2. Except for some narrow frequency regions waves tend to travel predominantly along either the host or the build-up in an asymptotic manner. The larger is the difference between the stiffnesses of the host waveguide and the accretion, the more the wave motion is decoupled. If a wave follows the host asymptote, it resembles behaviour of a free-free host waveguide that is almost entirely decoupled from the build-up. In this case the shear stress at the interface tends to be very low, following the traction-free boundary condition. In contrast, when a wave follows the accretion asymptote, the waveguide behaves as a clamped-free build-up, i.e. the interface surface is almost rigid. Owing to the large difference between the stiffnesses of the two components, a very high interface shear stress is generated.

At first, build-up dominated waves seem suitable for invoking delamination. However, these waves carry most of the energy along the accretion as they tend to the uncoupled asymptotic solution. It is known that wave energy distribution is directly related to wave attenuation for elastic waveguides covered with a lossy layer (Simonetti 2004). As accretions often fall into this category, built-up dominated waves which provide high interface shear stress are strongly attenuated, and hence are not particularly useful for practical applications.

We demonstrate the above observations on an illustrative example of a 1 mm thick aluminium plate in plane strain covered with a 2 mm thick glaze ice accretion. The material properties used in the simulations are listed in Table 1.

Calculations were performed using the semi-analytical finite element method (SAFE) which is a well established method for obtaining the dispersion curves for one-dimensional waveguides (Hayashi et al. 2003; Bartoli et al. 2006). The method utilises an FE-like procedure for the cross-section discretisation and assumes the displacement to be harmonic along the propagation direction. To ensure accuracy, we used the global matrix method (Lowe 1995) to find the stress distributions from the previously computed dispersion curves as proposed by Gao (2007). In the SAFE calculations the aluminium layer was modelled with five and the ice layer with six 3-noded quadratic elements.

The results for both Lamb and SH waves are combined in Figure 3. Figure 3(a) shows the transverse shear stress at the interface normalised with respect to unit power flow across a one metre wide section of the waveguide (Kalkowski 2015). The corresponding phase velocity dispersion curves are presented in Figure 3(b) and the attenuation curves in Figure 3(c). Since the materials are assumed isotropic, Lamb (solid lines) and SH waves (dashed lines) are decoupled. To maintain consistency with widely used terminology the fundamental waves are labelled as A_0 (flexural), S_0 (compressional) and SH_0 (shear horizontal), although there is no symmetry or antisymmetry in the displacement distribution across the considered waveguide. A few frequency regions corresponding to the local stress maxima are highlighted in Figure 3 for discussion.

At low frequencies (i.e. when the compressional wave is non-dispersive), the flexural wave is the most effective in generating interface shear stress. Although up to ca. 42 kHz it carries a significant proportion of the energy along the accretion, the attenuation is still reasonably low (although higher than for the SH_0 and the S_0 waves). The SH_0 wave is associated with a slightly higher stress than the S_0 wave, yet considerably lower than the flexural wave up to ca. 400 kHz.

The peaks in interface stress occur around the cut-off frequencies of the higher-order waves. Yet, as they propagate energy predominantly along the accretion, they are classified as build-up dominated, which indicates that they are heavily attenuated as shown in Figure 3(c).

Wave attenuation is dictating the frequency limit of the applicability of ultrasonic accretion removal. The flexural wave provides 36 $\mathrm{kPa}/\sqrt{\mathrm{W/m}}$ at around 90 kHz with an attenuation of 10 $\mathrm{dB\,m^{-1}}$. Whilst high frequency waves can generate higher stresses, their attenuation is at least an order of magnitude higher (assuming constant loss factor of the accretion material). Consequently, analysing the behaviour at hundreds of kilohertz provides some interesting physical insight but seems not to be very relevant to practical implementation.

Wave-based model for piezoelectric excitation

Qualitative outcomes from the free wave analysis can be revisited and enriched by introducing a realistic excitation mechanism. The adopted modelling approach is briefly reviewed in this section and any further details can be found in our previous work (Kalkowski 2015; Kalkowski et al. 2016).

A waveguide with accretion is modelled in the wave domain using semi-analytical finite elements and analytical wave scattering/reflection relationships. The key idea is to treat a multi-component one-dimensional waveguide as composed of finite sections of uniform waveguides called wave elements hereafter. In the first step, the structure is subdivided into multiple wave elements. Then, the wave characteristics of each wave element (wavenumbers, wave mode shapes) and excited wave amplitudes (for elements including PZT actuators) are found using the semi-analytical finite element method.

Whilst the SAFE method is used widely for calculating dispersion curves, it was recently extended to include materials with piezoelectric coupling enabling the calculation of piezo-excited waves in the wave domain directly with no need for any assumption on the dynamics of the actuator or its mutual interaction with the structure (Kalkowski et al. 2016).

The wave elements are coupled using wave scattering relationships obtained from the wave mode shapes (Harland et al. 2001). Any desired response is calculated straightforwardly in the final step using matrix algebra.

The adopted modelling technique has the following advantages over other established models for piezoelectric excitation: firstly, the dynamics of the actuator are included

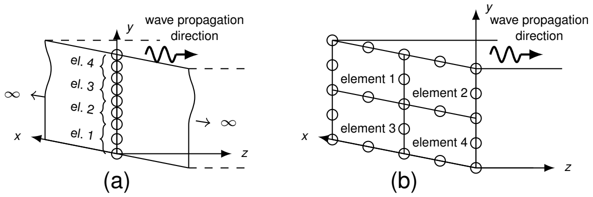

(a) (b)

Figure 4. Schematic description of the cross-section configurations considered in this paper: (a) a 1D cross-section; (b) a 2D cross-section.

and no assumption is made on its interaction with the structure. Secondly, all calculations including piezoelectric excitation are conducted in the wave domain using one electromechanical model. Waveguides of an arbitrary cross-section can be considered; this means that three-dimensional deformation can be modelled, assuming that the wave propagates along one direction (this is not achievable using the pin-force model limited by plane stress/strain formulations). Finally, the model can be formulated in a versatile piece-wise manner (Kalkowski 2015) for complex built-up waveguides.

Piezo-induced interface shear stress

In this section we present the numerical results for piezo-induced interface shear stress for illustrative cases. To investigate the effect solely of incident waves, we focus on structures of an infinite extent in the direction of propagation (z).

Two configurations of the host structure were considered (see schematic description in Figure 4): (i) a 1 mm thick aluminium plate in plane strain (represented by 1D finite elements – 1D cross-section) and (ii) a 24 × 1 mm aluminium rectangular beam (represented by 2D finite elements – 2D cross-section). The former provides a direct link to the free wave analysis from the previous section and some general insight that is useful for understanding the underlying phenomena. The latter is a simple structure that can easily be verified experimentally, and hence, raises issues that are expected to be encountered in real scenarios. Material properties used throughout this paper are gathered in Table 1 and Table 2.

Table 1. Properties of the isotropic materials used in the paper (ice after Gao and Rose (2009)), where E is the Young's modulus and ν is the Poisson ratio, ρ is the density and η is the loss factor.

material	E, GPa	ν	ρ, kg m^{-3}	η
aluminium	70	0.3	2700	0.002
steel	163	0.3	8000	0.0001
silvered epoxy	15	0.4	1000	0.0001
glaze ice	8.3	0.351	900	0.01

Table 2. Properties of Noliac NCE40 PZT ceramics: $\mathbf{C}^{\mathrm{E}}$ is the stiffness matrix under the short-circuit condition, $\mathbf{e}$ is the piezoelectric stress coefficient matrix, ε^{ϵ} is the permittivity matrix at zero-strain condition.

Property	value
ρ, kg m^{-3}	7850
η	0.007
$c^E_{xxxx} = c^E_{zzzz}$, GPa	126.35
$c^E_{xxyy} = c^E_{yyzz}$, GPa	58.68
c^E_{yyyy}, GPa	99.88
c^E_{xxzz}, GPa	62.93
c^E_{xzxz}, GPa	31.71
$c^E_{yzyz} = c^E_{xyxy}$, GPa	36.77
$\varepsilon^{\epsilon}_{xx} = \varepsilon^{\epsilon}_{zz}$, nF m^{-1}	5.5
$\varepsilon^{\epsilon}_{yy}$, nF m^{-1}	5.196
$e_{y,xxxx} = e_{y,zzzz}$, N V^{-1} m^{-1}	-3.239
$e_{z,yzyz} = e_{x,xyxy}$, N V^{-1} m^{-1}	13.075
$e_{y,yyyy}$, N V^{-1} m^{-1}	16.335

Predicting stress at the interface of two layers of different properties is not a straightforward task in displacement-based FE on which SAFE is based. To represent stress accurately, the mesh needs to be much finer than indicated by typical convergence criteria. Depending on the structural configuration the following measures were adopted to ensure that our predictions are realistic.

For 1D cross-sections, as mentioned in the free wave example, we used the SAFE/wave model to solve the problem for travelling wave amplitudes and then employed an analytical formulation based on the global matrix method (Lowe 1995) to extract an exact distribution of the stress field using the previously computed wave amplitudes as proposed by (Gao 2007). In the 1D model we used six 1D quadratic elements through the thickness of the ice layer and five such elements through the thicknesses of the both the aluminium and piezoelectric layers.

For 2D cross-sections, no general analytical formulation for stress distribution is available. Therefore, the predictions

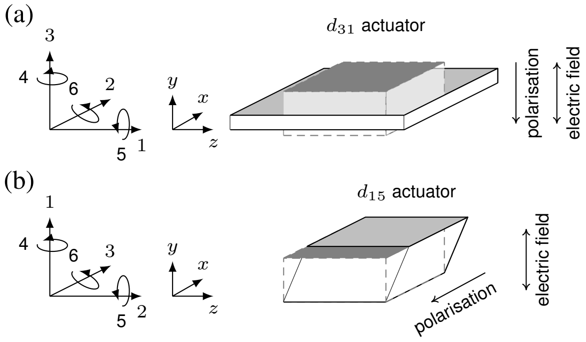

Figure 5. Types of PZT actuators studied and their modes of operation: (a) d_{31}; (b) d_{15}.

were validated against a benchmark with a very fine mesh at a few peak frequencies. The results were accepted if the computed resultant stresses were within a chosen threshold of the benchmark case. For the purpose of a subsequent experimental validation the threshold was chosen to be 1 dB. Given the uncertainties in the accretion material properties, bond quality and dimensions, uncertainties in the experimental data far exceed convergence errors in the model. In this section, 2D cross-sections were meshed with 14 quadrilateral biquadratic elements across the width of the beam for each layer; both aluminium and ice layers with five elements through the thickness, whereas the epoxy and actuator layers with one and two elements through the thickness, respectively.

To cover all basic types of waves propagating in plate-like structures, we studied two types of piezoelectric actuators: d_{31} and d_{15} (see Figure 5). The former is the most common configuration in which the poling direction (y) coincides with the direction of application of the electric field. Hence, d_{31} and d_{33} coefficients are active and the actuator is expected to excite Lamb-like waves. A d_{15} actuator is poled along the width (x) direction with the electric field applied across the thickness (y) direction. Consequently, electrical driving of the actuator activates predominantly the shear mode capable of triggering SH waves (for 1D cross-section) or torsional waves (for 2D cross-section) waves. Note that the notation for the indices refers to the most common convention, which assumes ‘3’ to be the poling direction.

Interface stress response for an infinite plate in plane strain (1D cross-section)

In this section the response of an aluminium/ice (1 mm/2 mm) plate excited by a piezoelectric actuator modelled in plane strain is analysed. We look at the transverse shear stress at the interface associated with incident waves at 0.1 m from the edge of the actuator (0.05 × 0.002 m, NCE40).

A d_{31} actuator – Lamb waves The superimposed interface shear stress (σ_{yz}) induced by a d_{31} actuator driven with a harmonic voltage of amplitude 1 V (called stress FRF hereafter) is presented in Figure 6(a). Throughout most of the frequency range a typical pattern of peaks and valleys arising from the relationship between the length of the actuator and the predominantly excited wavelength can be observed. An immediately noticeable feature are the two global peaks at 440 and 790 kHz. To further explain it, the electrical impedance of the actuator is plotted on the secondary y-axis in Figure 6(a) and the dispersion curves for the NCE40/aluminium/ice section of the plate – in Figure 6(b).

The electrical impedance of the actuator incorporates the imprints of the mechanical response via the electromechanical coupling. Close to the frequencies where an odd multiple of half-wavelengths matches the length of the actuator, its electrical impedance becomes predominantly real. This is an optimal condition for the excitation of the waveguide, as it appears to the actuator as an energy absorber. These resonances are referred to as ‘along-length’ resonances. Yet, the predominantly capacitive nature of the actuator renders this effect hardly noticeable in the magnitude of the impedance. The local peaks of the stress FRF, although not associated with clear dips of the electrical impedance, are most often along-length resonances.

The other class are the cross-sectional resonances which are related to the cut-off frequencies of higher-order waves in the actuator-structure waveguide. Cut-off frequencies are essentially the resonances of the cross-section of the waveguide. Whenever the deformation associated with a particular cut-off frequency couples well with the electric field applied over the electrode, the actuator is at a coupled electromechanical resonance. Under the plane strain assumption, the cross-sectional resonances of d_{31}

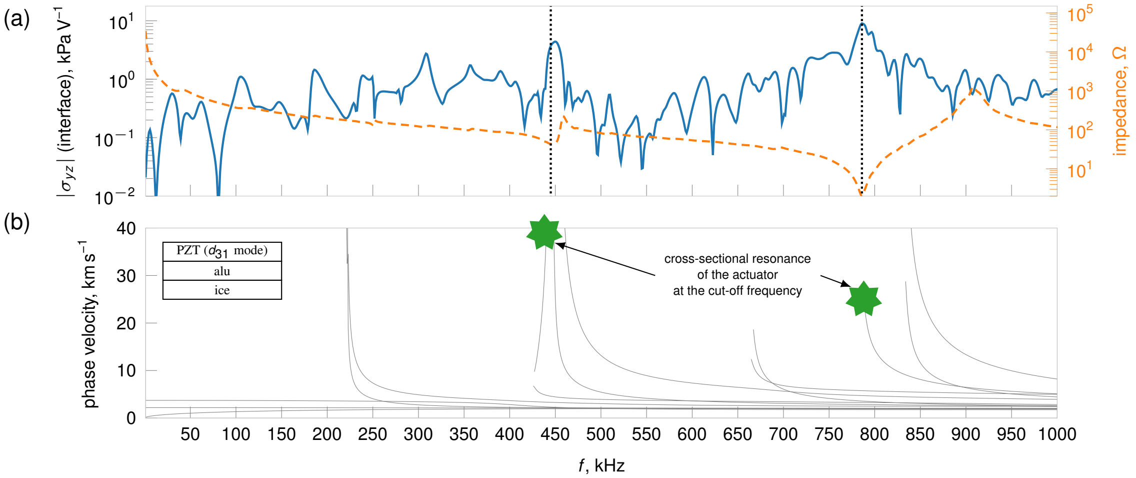

Figure 6. Interface shear stress for an aluminium (1 mm) – glaze ice (2 mm) plate excited by a d_{31} actuator: a) stress FRF (solid line) and the electrical impedance of the actuator (dashed line); b) dispersion curves in the NCE40/aluminium/ice plate.

actuators are related to the so called thickness-stretch modes (symmetric deformation), whereas those of the d_{15} actuators – to thickness-shear modes (anti-symmetric deformation) – see Graff (1991) for reference on the cut-off frequencies resonance modes. These cut-off frequencies refer to the whole cross-section composed of the actuator layer and the host structure, not the actuator on its own.

The global stress peaks at ca. 440 kHz and 790 kHz in Figure 6(a) correspond to the dips of the electrical impedance (cross-sectional resonances) associated with two of the cut-off frequencies in the actuator-covered section – marked in Figure 6(b). As the actuator is driven at resonance, it induces maximum stress.

Magnitudes of particular wave contributions to the superimposed stress are presented in Figure 7(a), and the corresponding dispersion curves for an aluminium/ice plate are shown in Figure 7(b). As expected, none of the SH-type waves (dotted lines) is triggered by a d_{31} actuator.

At low frequencies, the flexural wave (A_0) generates the highest interface stress. The contribution of the S_0 wave (compressional at low frequencies) grows with frequency and becomes comparable to that of the A_0 wave over ca. 170 kHz. Despite having the potential for generating high stress, higher-order waves at or very close to their cut-off frequencies are rather weakly excited and suffer from large attenuation. Global stress maxima are hence not related to the cut-off frequencies of waves in the iced plate, but to the resonances of the actuator. Therefore, including the effect of its dynamics in the model is vital for the considered application.

d_{15} *actuator – SH waves* We now look at the interface shear stress induced by a d_{15} actuator. As in the previous section, the superimposed interface shear stress (σ_{xy}) response is presented together with the electrical impedance of the actuator in Figure 8(a). The dispersion curves for the NCE40/aluminium/ice section of the plate are shown in Figure 8(b).

The global stress peaks correspond to the dips of the electrical impedance (cross-sectional resonances of the actuator) associated with the cut-off frequencies in the actuator-covered section. A d_{15} actuator triggers only SH waves and couples well with thickness-shear cut-off resonances.

Magnitudes of particular wave contributions to the superimposed interface shear stress are presented in Figure 9(a) and the corresponding dispersion curves for an aluminium/ice plate are shown in Figure 9(b). There are three SH waves in the frequency range considered. At very low frequencies the fundamental SH wave generates very low interface stress which gradually increases up to the maximum at 223 kHz. After the higher-order SH wave starts to propagate, it prevails in the stress response with a maximum at 458 kHz. It is emphasised again that the global

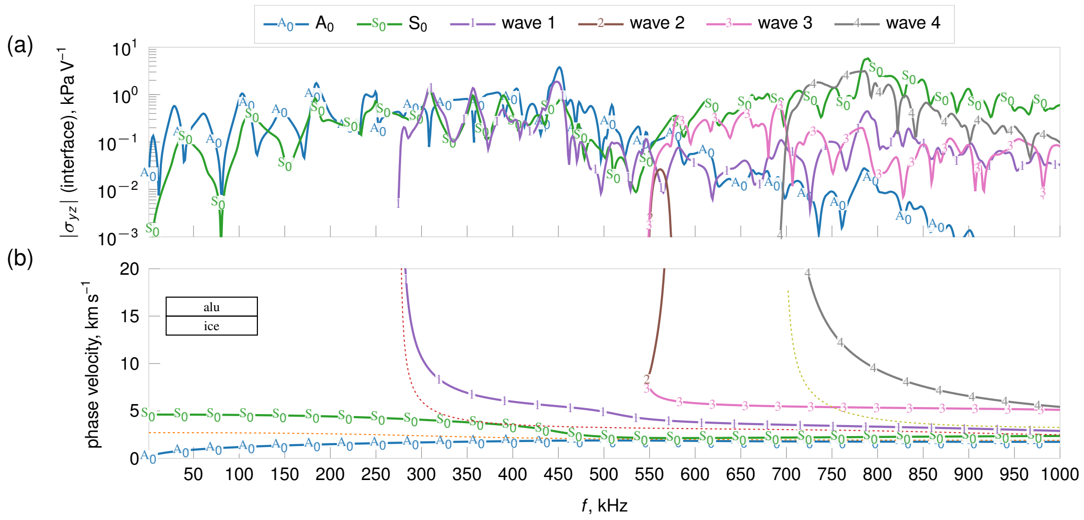

Figure 7. Interface shear stress and dispersion curves for an aluminium (1 mm) – glaze ice (2 mm) plate excited by a d_{31} actuator: a) wave contributions to the overall interface shear stress; b) dispersion curves (dotted lines – SH waves).

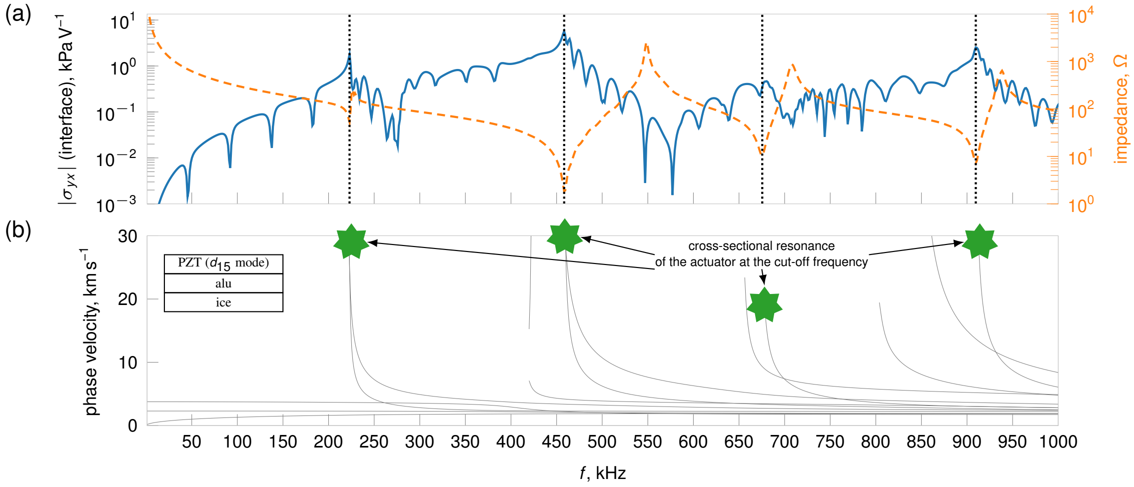

Figure 8. Interface shear stress for an aluminium (1 mm) – glaze ice (2 mm) plate excited by a d_{15} actuator: a) stress FRF (solid line) and the electrical impedance of the actuator (dashed line); b) dispersion curves in the NCE40/aluminium/ice plate.

maxima of the response are dictated predominantly by the dynamics of the actuator.

Electrical power requirement A critical quantity describing the applicability of wave-based ultrasonic accretion removal is the electrical power requirement. Our wave model enables the power consumed by the PZT actuator to be extracted. However, since the actuator is a complex electrical load the power transfer issues have to be accounted for. The efficiency of the electrical power transfer between an ultrasonic source (amplifier) and a receiver (actuator) depends on the impedances of these elements.

At frequencies of interest the electromagnetic wavelength is very large, hence the system can be represented by a simple lumped parameter circuit (Figure 10), where $v_S = V_s \exp\left(\jmath\omega t\right)$ is the time-harmonic voltage of the Thévenin's equivalent voltage source, Z_S is the impedance of the source and Z_L is the impedance of the load. The voltage across the load v_L and the current i flowing through it can be calculated as

$$v_L = v_S \frac{Z_L}{Z_L + Z_S} \qquad \text{and} \qquad i = v_S \frac{1}{Z_L + Z_S} \tag{1}$$

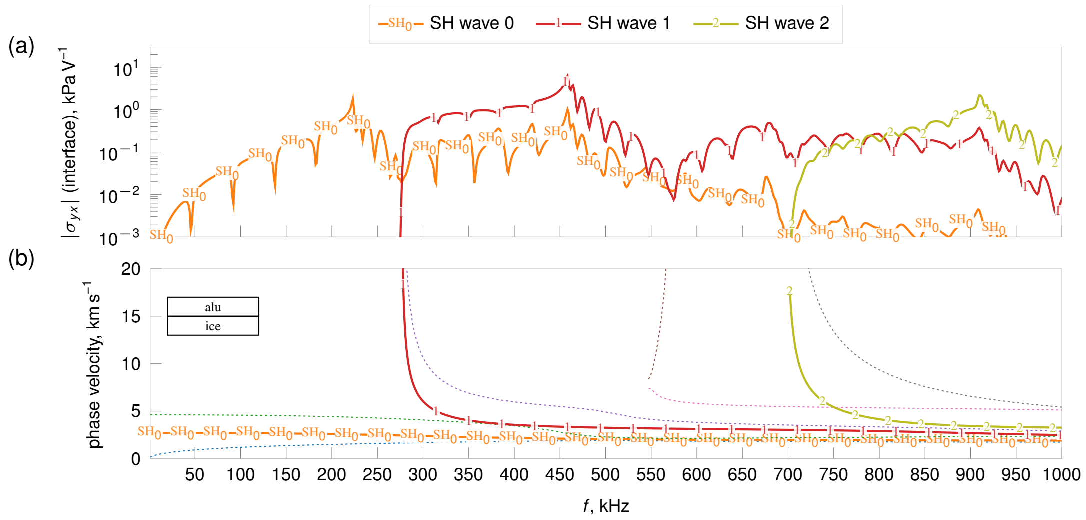

Figure 9. Interface shear stress and dispersion curves for an aluminium (1 mm) – glaze ice (2 mm) plate equipped with a d_{15} actuator: a) wave contributions to the overall interface shear stress; b) dispersion curves (dotted lines – Lamb waves).

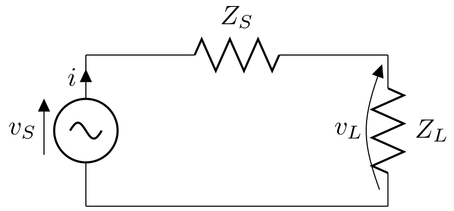

Figure 10. Lumped parameter circuit representing the power source–actuator system.

The time-average of the power absorbed by the actuator is obtained from

$$P_R = \frac{1}{2}\mathrm{Re}\{V_L I^*\} = \frac{1}{2}|V_S|^2 \frac{\mathrm{Re}\{Z_L\}}{|Z_L + Z_S|^2} \qquad (2)$$

where V_L, I and V_S are the complex amplitudes of the respective time-harmonic quantities. Equation (2) indicates that power transfer is maximum if the impedance of the load is the conjugate of the impedance of the source. This is often not the case for a frequency dependent actuator impedance. To make the power from equation (2) available to the load, the amplifier needs to be capable of delivering considerably more power. As for complex loads, the power rating of the amplifier is a practical measure. Thus, a required power capability of the amplifier is defined here as the power rating of the amplifier with output impedance Z_S that ensures delivery of certain active power P_R to the load of impedance Z_L:

$$P_c = \left| \frac{Z_L + Z_S}{\mathrm{Re}\{Z_L\}} \right| P_R \qquad (3)$$

Although the active power consumed by the actuator provides the physical understanding of the power transduction process, the power capability of a driving source with a fixed impedance is a more practical measure indicating how powerful the amplifier needs to be.

The interface shear stress generated by the piezoelectric actuation is presented with reference to those power quantities in Figure 11. For calculation of the electrical power some arbitrary width of the actuator has to be chosen in the plane strain model. Here, the results were scaled so that they represent a 20 mm wide strip. For the calculation of P_c it was assumed that the driving source output impedance is 50 Ω (standard for off-the-shelf equipment).

For most of the frequency range in the chosen illustrative example, the d_{31} actuator performs better than the d_{15} counterpart, particularly at low frequencies. The stresses with reference to the power source capability are significantly lower than those with reference to power absorbed by the actuator. It is also suggested from Figure 11 that with frequency increasing into the high ultrasonic region, piezoelectric excitation becomes notably

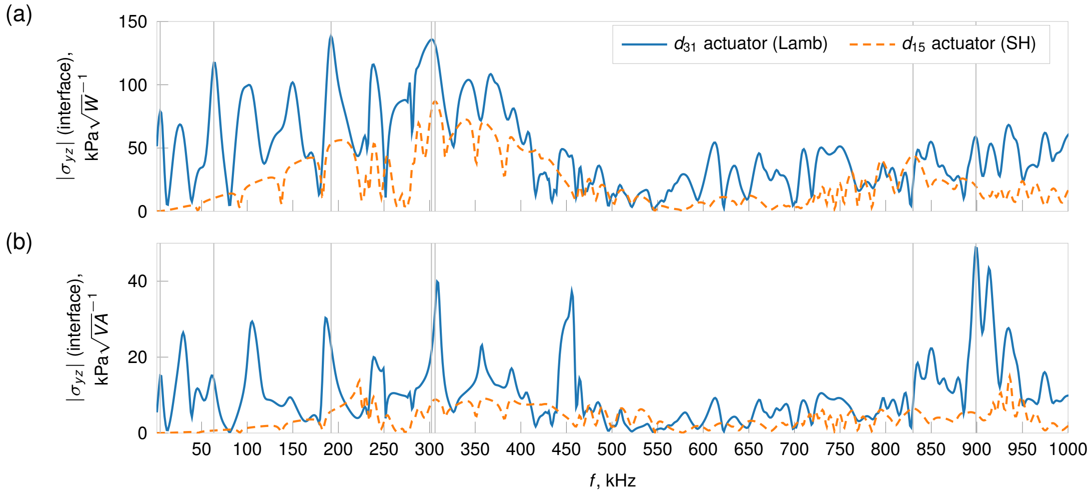

Figure 11. Interface shear stress with respect to the electrical power in an aluminium (1 mm) – glaze ice (2 mm) plate equipped with a Noliac NCE40 actuator: a) active (real) power; b) power capability of a 50 Ω source.

Table 3. Electrical power requirements for breaking the static ice/aluminium shear adhesion strength (1.5 MPa) at chosen frequencies from Figure 11.

	d_{31} actuator		d_{15} actuator	
f (kHz)	P_R (kW)	P_c (kVA)	P_R (kW)	P_c (kVA)
4.6	0.36	9.79	$> 10^3$	$> 10^3$
63.4	0.16	11.16	20.77	$> 10^3$
191.8	0.12	4.18	0.79	68.80
302.3	0.12	4.74	0.35	34.61
305.9	0.13	2.23	0.30	28.85
830.3	3.78	29.37	1.16	53.44
898.7	0.65	0.94	5.66	85.64

less effective in generating interface shear stress. Note that the piezoelectric actuator is assumed to be linear in all cases considered in this paper.

Assuming the strength of the aluminium–glaze ice bond σ_b to be 1.5 MPa (Palacios and Smith 2008), the power requirements for de-icing at a few frequencies marked with grey vertical lines in Figure 11 are presented in Table 3.

The powers indicated by Table 3 appear to be practically non-realisable. From the active power perspective the most effective frequencies are 191.8 and 302.3 kHz, requiring 120 W to be consumed by the actuator for inducing debonding. Power capability of a 50 Ω driving source would need to be almost 4.18 and 4.74 kW, respectively, which put the practicability of the approach in question.

However, two additional aspects need to be accounted for. Firstly, the bond strength used in this paper was obtained statically (Palacios and Smith 2008) and is expected to be higher than the dynamic bond strength. Secondly, the power capability is calculated for a 50 Ω source only (the typical off-the shelf characteristics). A dedicated system could have different output impedance adjusted to match the structural configuration, which can possibly lower the P_c indications. Finally, an infinite plate in plane strain is an abstract idealisation which may not be representative for many practical cases. In fact, components susceptible to accretions (such as the aircraft wing leading edge) can be modelled as 1D waveguides with finite (2D) cross-sections. Among other features, higher-order waves in such structures appear at much lower frequencies which may be important from the viewpoint of wave-based accretion removal and hence is discussed in the next section.

Interface stress response for a beam-like waveguide (2D cross-section)

In this section we look at the interface stress generated in a rectangular beam. Although the waveguide is somewhat simplistic and theoretical, the important physical phenomena from the viewpoint of delaminating accretions can be observed well in this case and applied to practical structures such as a leading edge profile or a turbine blade. The actuator (0.076 × 0.024 × 0.0022 m Noliac NCE40) is bonded to the beam via a 0.1 mm thick epoxy layer and covers its whole width. The response is analysed at 0.164 m from the actuator.

The cross-section of the waveguide is now finite hence, all stress components can be excited and they are allowed to vary over the cross-section plane. To quantify the effect of piezoelectric excitation in a reasonably practical way, we chose to compare the maximum resultant interface transverse shear stress $\sigma_\tau = \sqrt{\sigma_{yz}^2 + \sigma_{xy}^2}$ across the width of the beam excluding the near-edge region.

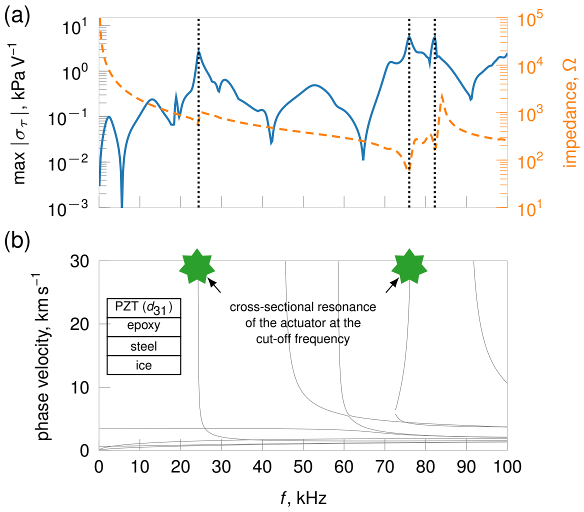

Figure 12. Interface shear stress and dispersion curves for a 24×1 mm aluminium beam covered with 2 mm thick glaze ice accretion and equipped with a d_{31} actuator: a) stress FRF (solid line) and the electrical impedance of the actuator (dashed line); b) dispersion curves in the NCE40/epoxy/aluminium/ice beam.

d_{31} *actuator* The results for the superimposed interface stress, the electrical impedance of the d_{31} actuator and the dispersion curves for a PZT-covered section are shown in Figure 12. We observe the typical pattern of peaks and valleys at low frequencies and three well pronounced stress maxima at 24, 76 and 82 kHz. These peaks are associated with the dips of the electrical impedance of the actuator indicating that it is operating at resonance. The first two resonances in Figure 12(a) are cross-sectional and correspond to the cut-off frequencies associated with wave mode shapes that are symmetric about the y-axis (see Figure 12(b)). The third resonance does not align with any of the actuator cross-sectional resonances and will be explained later.

The interface stress associated with particular waves is plotted in Figure 13. To clarify the comparison the wave solutions have been tracked so that they represent the same deformation pattern along a dispersion curve. In a general elastic waveguide the dispersion curves never cross (even if their projections on the real wavenumber axis may appear to) as all the degrees of freedom are coupled via Hooke's law. Owing to our somewhat non-physical 'mode tracking' procedure, the stress response can appear discontinuous when the dispersion curves come close to each other.

At low frequencies the interface shear stress is generated predominantly by the fundamental flexural wave (Figure 13). The first higher-order wave (across-width bending) cuts off at around 17 kHz and dominates the response up to around 26 kHz. The global stress peak around 24 kHz is related to the cut-off frequency of the same higher-order wave (across-width bending) in the PZT-covered section. These effects are very notable for the generated interface stress and cannot be captured by simplified approaches such as the pin-force model.

The preceding peak at around 18 kHz appears to be related to the apparent crossing of the longitudinal ('L$_0$') and the across-width bending ('U') waves – see Figure 13(b). The stress peaks may occur close to points where dispersion curves come close (so called repulsive points) (Kalkowski et al. 2012).

Up to 75 kHz only the fundamental flexural wave and the first higher-order ('U') wave invoke non-negligible interface shear stress. The contribution of the compressional wave becomes significant around 75 kHz. The second global peak at 76 kHz related to the cross-sectional resonance of the actuator is governed predominantly by the flexural wave. The last significant peak at 82 kHz appears again very close to the frequency at which the 3rd across-width bending ('W') dispersion curve comes close to the 2nd flexural 'Z' dispersion curve in Figure 12(b).

Although it is clear that some deformation patterns are more likely to generate higher interface stress than others, the dynamics of the actuator – the location of the resonances and how efficiently they transmit into particular waves in

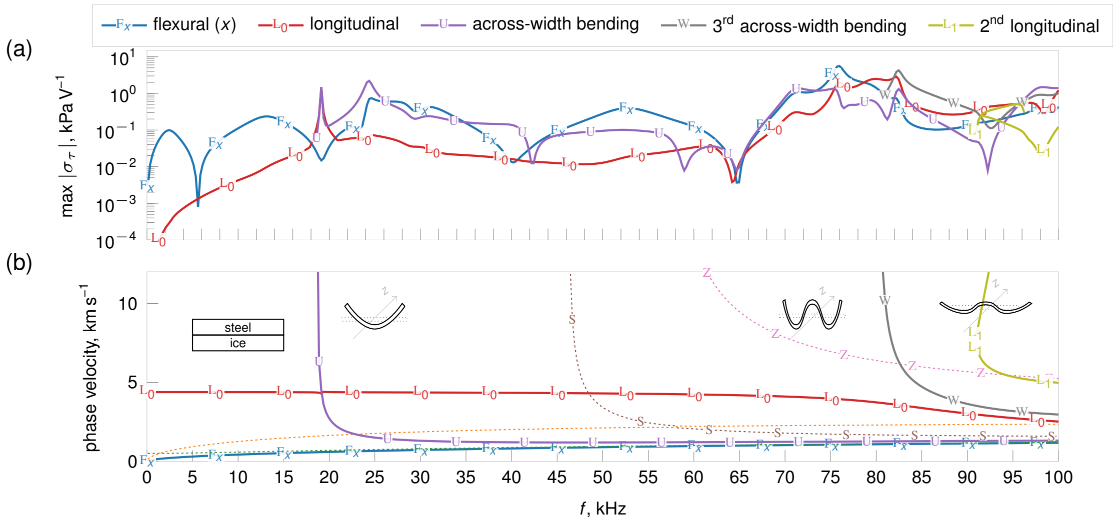

Figure 13. Wave composition of the interface shear stress a 24×1 mm aluminium beam covered with 2 mm thick glaze ice accretion and equipped with a d_{31} actuator: a) wave contributions to the overall interface shear stress; b) dispersion curves (dotted lines represent waves that are not excited).

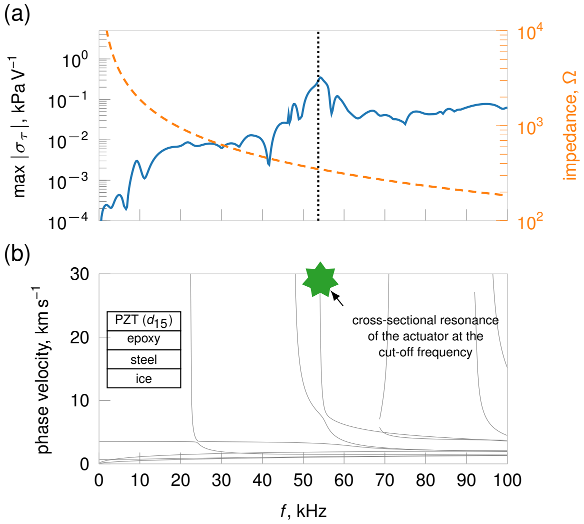

Figure 14. Interface shear stress and dispersion curves for a 24×1 mm aluminium beam covered with 2 mm thick glaze ice accretion and equipped with a d_{15} actuator: a) stress FRF (solid line) and the electrical impedance of the actuator (dashed line); b) dispersion curves in the NCE40/epoxy/alu/ice beam.

the accretion-covered waveguide – play a key role in the effectiveness of delaminating accretions.

d_{15} *actuator* The superimposed interface stress response to a d_{15} actuator excitation together with the electrical impedance of the actuator and the dispersion curves of the actuator-covered section are presented in Figure 14. The induced stress is small at low frequencies (around an order of magnitude smaller than for a d_{31} actuator) and gradually increases towards the only global peak at around 54 kHz associated with a cut-off frequency. Within the considered frequency range, there is only one higher-order wave in the actuator-covered section which couples with the applied electric field at its cut-off frequency, although the dip in the impedance is very shallow.

The wave composition of the response is presented in Figure 15. A d_{15} actuator excites waves for which the deformation pattern is antisymmetric about the y-axis. Apart from the torsional and flexural (around the y-axis) fundamental waves, two higher-order waves are excited. At low frequencies the interface shear stress arises predominantly from the fundamental torsional wave. The global stress peak at 54 kHz is generated mainly by the 2nd across-width bending wave.

Electrical power requirement We now look at the generated interface stress with reference to electrical power quantities. The comparison of the stress generation efficiency for d_{31} and d_{15} actuators is shown in Figure 16. Firstly, we note that over most of the considered frequency range a d_{31} actuator provides significantly higher interface shear stress than its d_{15} counterpart. The only notable

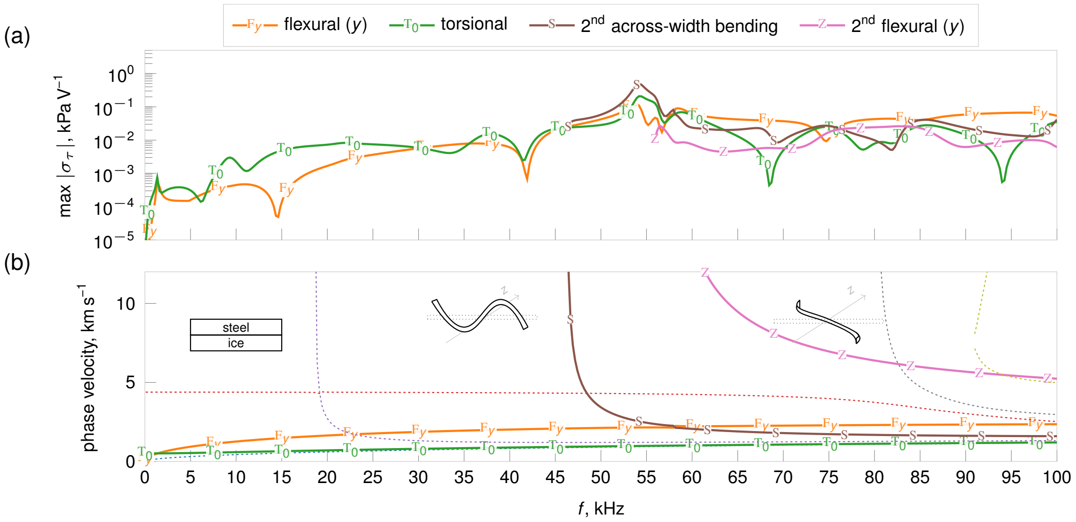

Figure 15. Wave composition of the interface shear stress a 24×1 mm aluminium beam covered with 2 mm thick glaze ice accretion and equipped with a d_{15} actuator: a) wave contributions to the overall interface shear stress; b) dispersion curves (dotted lines represent waves that are not excited).

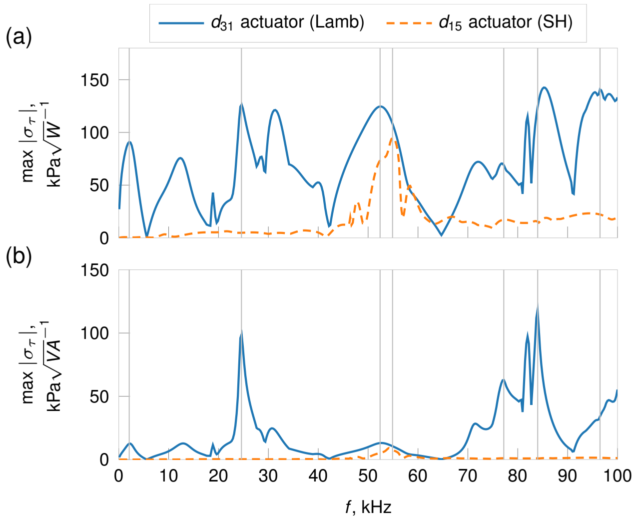

Figure 16. Interface shear stress with respect to the electrical power in a 24×1 mm aluminium beam covered with 2 mm thick glaze ice accretion and equipped with a Noliac NCE40 actuator: a) active (real) power; b) power capability of a 50 Ω source.

peak for the d_{15} actuator occurs close to its cross-sectional resonance near 54 kHz.

Implications of the electrical power transfer and electrical-to-mechanical transduction can well be observed in Figure 16. When a reference to the active power P_R is taken in Figure 16(a), multiple peaks occur. Some of them correspond to the global stress maxima from Figure 12 related to the cross-sectional resonances and others to the along-length resonances. The height of the peaks corresponding to both classes of resonances is comparable in Figure 16(a). However, far from cross-sectional resonances the electrical impedance of the actuator is largely reactive, hence delivering large power to such load is not a straightforward task.

The results in Figure 16(b) include the effect of power transfer between a standard electrical driving system and the actuator. The stress levels are now notably lower. The peak frequencies in Figure 16(b) correspond to the coincidence between high stress per absorbed power from Figure 16(a) and the optimal electrical power transfer between the source and the actuator. At those frequencies, it is possible to drive the actuator more efficiently and inject more power into the waveguide.

To provide reference to the de-icing problem, we compare respective power requirements for de-icing at a few frequencies marked with grey vertical lines in Figure 16 in Table 4. The strength of the ice bond was assumed to be 1.5 MPa and the driving source to have a 50 Ω output impedance.

Power requirements shown in Table 4 are excessively high from a practical perspective. In the most optimistic case at low frequencies, a d_{31} actuator requires a feasible

Table 4. Electrical power requirements for exceeding the static ice/aluminium shear adhesion strength (1.5 MPa) at characteristic frequencies from Figure 16 (local or global maxima)

	d_{31} actuator		d_{15} actuator	
f (kHz)	P_R (kW)	P_c (kVA)	P_R (kW)	P_c (kVA)
2.10	0.27	14.24	$> 10^3$	$> 10^3$
24.60	0.14	0.23	96.21	$> 10^3$
52.40	0.14	13.18	0.41	81.06
54.90	0.19	20.43	0.25	38.21
77.20	0.47	0.57	7.59	$> 10^3$
84.00	0.15	0.16	9.52	$> 10^3$
96.50	0.11	1.93	4.58	$> 10^3$

230 VA source, driving the actuator with 140 W. At high frequencies, a 1.9 kVA source driving the actuator with 110 W was found sufficient. These are far higher than a typical actuator could withstand. For a d_{15} actuator, the most promising is the peak at 54.9 kHz which requires 250 W to be delivered by a 38 kVA 50 Ω source.

However, a few factors need to be kept in mind. Firstly, the ice bond strength (static) reported in the literature is not consistent among the authors and varies from 0.1 to 1.6 MPa. It is worth noting that the dynamic deformation is expected to break the bond easier (but unfortunately no results on the dynamic strength of the bond are known to the authors). Moreover, in recent years considerable attention has been given to the development of specialised surface coatings which are 'accretion-phobic' (Menini and Farzaneh 2011; Farhadi et al. 2011). This, together with assuring high quality surface finish may lower the adhesion strength significantly. If the bond strength is halved, the power requirements drop by a factor of four.

The examples presented in this paper refer to the worst case scenarios, i.e. when no end reflections are present and when debonding is to be induced solely by an incident wave. In practice some reflections are always present, and even if weak, can significantly diminish power requirements. The interface stress values are structure-specific and some configurations facilitate achieving higher stress. The examples chosen in this paper aim to demonstrate the capabilities of the developed wave model for predicting interface stress resulting from piezoelectric actuation and give indications of the realistic power requirements for specific structures.

Experiment

This final section reports an experiment in which the effectiveness of piezo-actuated structural waves in delaminating surface accretions is demonstrated. Focusing on the effect of incident waves only, we endeavoured to emulate anechoic boundary conditions at the ends of a beam-like waveguide. This was achieved by placing them in boxes filled with sand in such a way that the thickness of the sand cover was gradually increased to ensure a smooth change in the mechanical impedance.

Experimental setup and accretion material

The experimental setup is shown schematically in Figure 17. We used a Noliac NCE40 actuator (0.024 × 0.0022 × 0.076 m - d_{31} mode) attached to a 24 mm wide, 3.42 mm thick and over six metres long steel beam. The actuator was powered by an RF amplifier (1020L, Electronics & Innovation Ltd.) driven by a waveform generator (TTi TGA1240). The amplifier is equipped with an LCD display on which the forward and reflected power readings are shown.

Piezoelectric excitation aimed to remove surface patches made of plaster. Plaster is known to be brittle and of Young's modulus similar to ice accretions. The commonly reported properties of ice are: Young's modulus – from 2.5 to 8.3 GPa, density – from 600 to 900 $\mathrm{kg\,m^{-3}}$ Gao and Rose (2009). Values reported by Vekinis et al. (1993) indicate that plaster can be a good alternative to ice for experiments in respect of its dynamic response. Choosing plaster enabled the difficulties associated with producing and handling ice to be circumvented, while keeping similar material characteristics in place. Moreover, the debonding is expected not to be significantly affected by elevated temperature resulting from actuator's vibration.

The shear adhesion strength of plaster was measured using a simple lap shear test to provide a reference for measurements. The breaking shear stress results are shown in Figure 18. For all cases the adhesion strength of plaster to aluminium is between 0.142 and 0.366 MPa. Although high variability corresponds well to the real-type accretion scenarios, it is difficult to quantify using simple tests. Nevertheless, results presented in Figure 18 were found

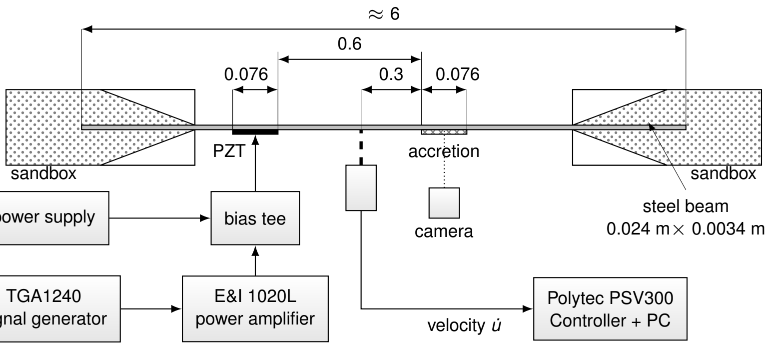

Figure 17. Experimental setup for the delamination demonstration.

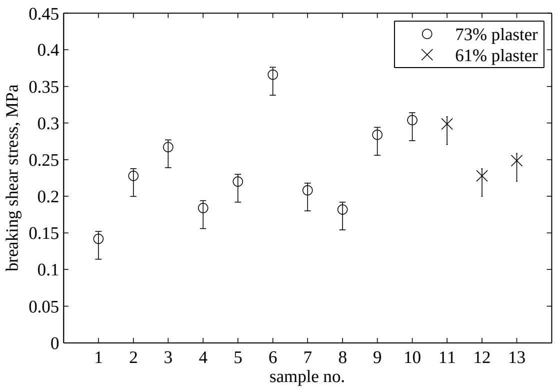

Figure 18. Shear adhesion strength of the plaster-aluminium bond: experimental results.

sufficient for the purpose of providing a reference for delamination experiments. Any further investigation on the bond strength is beyond the scope of this paper.

Simulated interface shear stress in a plaster-covered beam

The experiment was first performed numerically. The properties of the plaster (taken as isotropic) were assumed based on Vekinis et al. (1993) as follows: $E = 3$ GPa, $\rho = 1000\ \mathrm{kg\,m^{-3}}$, $\nu = 0.351$ and $\eta = 0.01$. The geometry and structural configuration for the considered case are shown in Figure 17, whereas the properties of steel and Noliac NCE40 material are listed in Table 1 and Table 2, respectively. The structure was modelled with 14 quadrilateral biquadratic elements across the width and with ten, four, two and one layer of elements through the thicknesses of the steel, ice, actuator and epoxy layers, respectively.

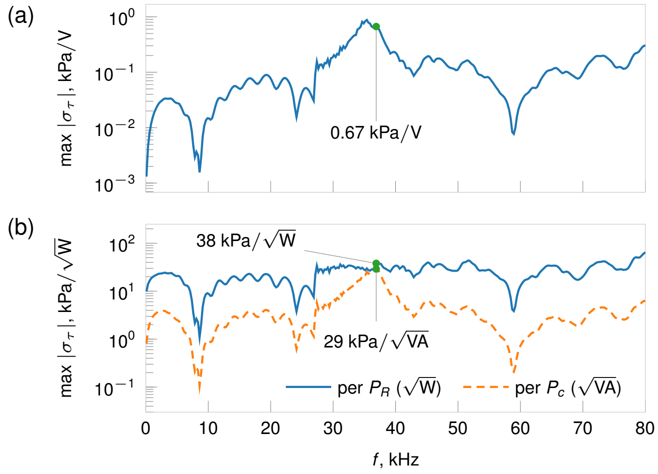

Figure 19. Numerical results for interface shear stress in a beam partially covered with 3 mm thick plaster accretion: (a) per voltage (b) per active power (solid line) and per power capability of a $50\ \Omega$ source (dashed line).

Simulation results for the interface shear stress with respect to voltage and electrical power are shown in Figure 19. As in the preceding section, we look at the maximum resultant transverse shear stress σ_τ along the width of the beam (excluding the near-edge region). The upper frequency limit of 80 kHz is dictated by the available equipment, however the observations from the preceding sections indicate that frequencies close to the first across-width bending cut-off frequency, which is within this range, are expected to be one of the most effective.

The required power capability of a $50\ \Omega$ driving source is in this case the most useful reference for analysing the results. As expected, the maximum achievable stress is associated with the first higher-order wave (across-width bending) cutting off in the PZT covered section around 36.9 kHz. The corresponding values for all chosen power reference quantities around that peak are listed in Figure 19.

The power requirements for delaminating plaster can be inferred from Figure 19. The simulations indicate that the ultrasonic action can be successful if the actuator consumes 40 (14–93) W of active power (values in parentheses correspond to the extreme values from Figure 18). It can be delivered to the actuator if a 50 Ω ultrasonic driving source is capable of producing 68 (24–159) VA (and handle the impedance mismatch). Note that as the properties of plaster were assumed and its thickness could not have been realised accurately in the lab, the aforementioned values serve as a guide only.

Procedure

Since PZT ceramics are much stronger in compression than in tension it is desirable to drive them predominantly in compression to avoid tensile cracks. In the experiment, a DC offset was applied to the output of the amplifier using a simple 'bias tee' circuit ensuring the tensile stress within the actuator to be minimised (Overmeyer et al. 2011).

The following experimental procedure was adopted. Firstly, at a low level of excitation, the optimal frequency was searched for around the 36.9 kHz resonance. It was identified based on the active power delivered to the actuator as indicated by the amplifier's display. Then, the driving power was increased up to the instant when plaster patch shedding was observed. For reference purposes, the surface velocity at a point equidistant from the actuator and the accreted patch was measured using a laser vibrometer for one of the experimental runs.

Results

The delamination was attempted in a few runs of which some conformed to the structural configuration showed in Figure 17 and the others did not (e.g. more patches were placed on the beam). The results indicating the active (consumed) power at the instant of delamination are listed in Table 5, and illustrative video snapshots showing the patches shedding are presented in Figure 20. Piezo-actuated structural waves were proven to be able to invoke delamination and remove the accretion.

Table 5. Electrical power consumed at the successful delamination attempts.

#	P_{FWD}	P_{RFD}	P_R (consumed)	as in Figure 17
1	83 W	63 W	20 W at 35.61 kHz	yes
2	52 W	32 W	20 W at 35.32 kHz	yes
3	93 W	56 W	37 W	no
4	130 W	81 W	49 W	no
5	18 W	8 W	10 W	no

After the patches had shed it was observed that some of them were only partially attached to the host beam, which made the debonding very difficult. Imperfect bonding between the layers significantly diminishes the generated interface stress which results in higher power requirements. We also noted that wave absorption at the boundaries was not ideal in the experimental rig, therefore the delamination experiment benefited from the effect of reflections albeit small in magnitude.

For the two runs for which the structural configuration was the same as in the simulations in Figure 17 the active power consumption at the delamination was measured to be 20 W. The corresponding numerical simulation indicates double that value. To quantify the correlation between the model and the experimental arrangement further, the surface velocity of the beam was monitored during the delamination in run 1 (see Table 5). The time history corresponding to the instant when the patch shed is shown in Figure 21(a). The relevant frequency domain numerical results computed using the developed wave model are presented in Figure 21(b).

Using the numerical data from Figure 21(b) one can calculate that if the actuator were driven with 20 W of active power, the surface velocity would be 202.6 mm/s. The observed surface velocity is 432.7 mm/s, which is more than twice the predicted value. This may be attributable to the residual reflections from the sandboxes which give rise to the response. If so, the interface shear stress generated by the 20 W ultrasonic actuation would be twice as high as predicted by the model. At 20 W of active power the model predicts the shear stress of 0.17 MPa at the interface. If one follows the observation that response is

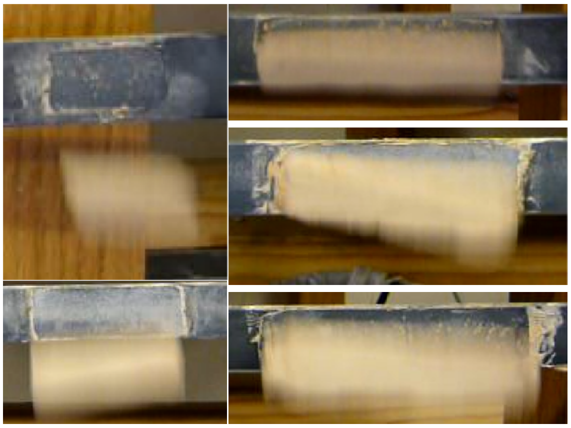

Figure 20. Video snapshots showing the plaster patches falling of the beam as a result of the ultrasonic actuation.

doubled compared to the numerical prediction, the interface shear stress generated in the experiment is estimated to be 0.34 MPa which is very close to the upper-bound values measured for plaster bond strength from Figure 18.

We emphasise that the properties of plaster were not measured and that our numerical predictions assume a perfect bond between the patch and the structure. Given the uncertainties in the experimental arrangement, analysis of which falls outside of the scope of this paper, it is acknowledged that piezo-actuated ultrasonic waves were demonstrated to be capable of removing surface accretion. The power requirements observed in the experimental demonstration were of an acceptable level and reasonably similar to those predicted by the numerical model (accounting for the differences explained above and the variability of shear adhesion strength). This confirms that the modelling technique demonstrated in this paper can be useful for a class of problems requiring computation of piezoelectric actuation including the effects of the actuator's dynamics. Finally, it shows the potential of high-frequency structural waves for delaminating unwanted build-ups in a scenario when the reflected waves are small.

Conclusions

In this paper the capability of piezo-excited structural waves for delaminating surface accretion was considered. Firstly, free waves in structures covered with accretions were discussed highlighting the importance of the weak coupling of the bilayer wave motion in such structures. High interface shear stress is often associated with accretion-dominated waves which are undesirable because of large attenuation. Hence, a trade-off between the two aforementioned conditions exists. It was also shown that waves associated with flexural deformation of the cross-section provide the highest interface shear stress.

Employing an excitation model in the wave domain that accounts for the dynamics of the actuator enabled calculating transfer functions between the generated stress and the applied voltage. The features of the numerical approach proved vital for modelling this application. Even at low ultrasonic frequencies the dynamics of the actuator played a critical role and the global stress maxima were found to be related to the actuator's resonances. Furthermore, a comparison between d_{31} and d_{15} actuators indicated that the former is more effective in generating high interface transverse shear stress.

The adopted modelling approach allowed for determining realistic electrical power requirements for delaminating accretions solely with incident waves. The illustrative results for ice on a thin aluminium plate suggest that achieving a desired effect with harmonic excitation and no end reflections (standing waves) may be impractical, although this is based on a static rather than dynamic adhesion strength of ice.

The electrical power transfer issues were also shown to be of critical importance. As the actuator can be driven by a single source effectively only at a limited range of frequencies, achieving high stress requires a careful choice of the driving system and the actuator together.

The paper concluded with an experimental demonstration of the concept and validation of the model. Piezo-actuated structural waves were proven capable of removing accretions from a waveguide with emulated anechoic terminations. Accounting for the issues discussed in the experimental section, the predicted power requirements corresponded reasonably well with the power consumption observed during the experiment.

Acknowledgements

The authors acknowledge the use of the IRIDIS High Performance Computing Facility, and associated services at the University

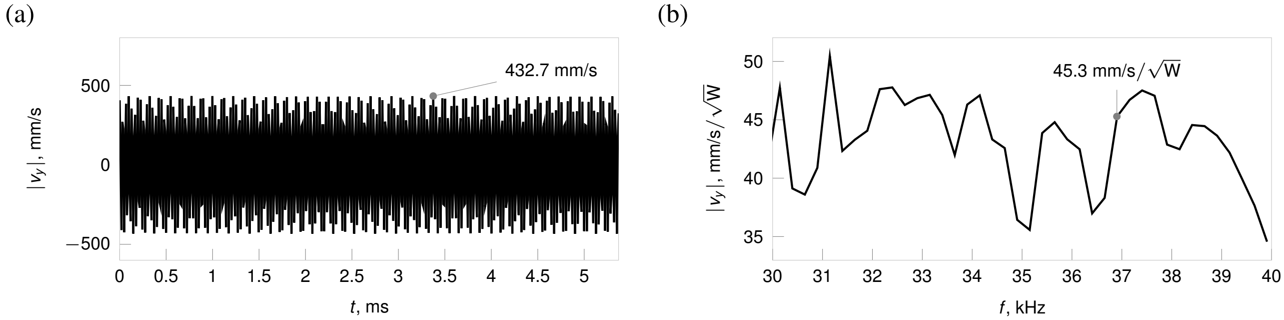

Figure 21. Surface velocity at the middle of the width of the steel beam: (a) time domain results recorded during the successful delamination attempt; (b) relevant frequency domain numerical results with respect to the active power.

of Southampton. We also thank the Stack Overflow online community for support in preparing associated software tools.

The data supporting this study are openly available from the University of Southampton repository at http://dx.doi.org/10.5258/SOTON/388188.

Funding

This research was possible thanks to the University of Southampton Postgraduate Research Studentship Programme. Financial support of Structural Funds in the Operational Programme Innovative Economy (IE OP) financed from the European Regional Development Fund – Project 'Modern material technologies in aerospace industry', Nr POIG.01.01.02-00-015/08-00 is gratefully acknowledged.

References

Adachi K, Saiki K and Sato H (1998) Supression of Frosting on a Metal Surface Using Ultrasonic Vibrations. *Proceedings of the IEEE Ultrasonics Symposium* : 759–762.

Bartoli I, Marzani A, Lanza di Scalea F and Viola E (2006) Modeling wave propagation in damped waveguides of arbitrary cross-section. *Journal of Sound and Vibration* 295(3-5): 685–707.

Borigo CJ (2014) *A novel actuator phasing method for ultrasonic de-icing of aircraft structures*. PhD Thesis, Pennsylvania State University.

Chu MC and Scavuzzo RJ (1991) Adhesive Shear Strength of Impact Ice. *AIAA Journal* 29: 1921–1926.

DiPlacido N, Soltis J, Smith EC and Palacios JL (2013) Enhancement of Ultrasonic De-Icing via Transient Excitation. In: *Proceedings of the 2nd Asian/Australian Rotorcraft Forum and The 4th International Basic Research Conference on Rotorcraft Technology*. Tianjin, China.

Farhadi S, Farzaneh M and Kulinich SA (2011) Anti-icing performance of superhydrophobic surfaces. *Applied Surface Science* 257(14): 6264–6269.

Gao H (2007) *Ultrasonic guided wave mechanics for composite material structural health monitoring*. PhD Thesis, Pennsylvania State University.

Gao H and Rose JL (2009) Ice Detection and Classification on an Aircraft Wing with Ultrasonic Shear Horizontal Guided Waves. *IEEE Transactions on Ultrasonics, Ferroelectrics, and Frequency Control* 56(2): 334–344.

Graff KF (1991) *Wave Motion in Elastic Solids*. Dover.

Harland NR, Mace BR and Jones RW (2001) Wave propagation, reflection and transmission in tunable fluid-filled beams. *Journal of Sound and Vibration* 241(5): 735–754.

Hayashi T, Song WJ and Rose JL (2003) Guided wave dispersion curves for a bar with an arbitrary cross-section, a rod and rail example. *Ultrasonics* 41(3): 175–183.

Kalkowski MK (2015) *Piezo-actuated structural waves for delaminating surface accretions*. PhD Thesis, University of Southampton.

Kalkowski MK, Rustighi E and Waters TP (2012) Wave based method for inducing delamination at the interface of a layered structure - feasibility study. In: *25th ISMA International converence of Noise and Vibration Engineering*. Leuven, Belgium.

Kalkowski MK, Rustighi E and Waters TP (2016) Modelling piezoelectric excitation in waveguides using the semi-analytical finite element method. *Computers & Structures* (accepted - in press). DOI:10.1016/j.compstruc.2016.05.022.

Li D and Chen Z (2014) Experimental study on instantaneously shedding frozen water droplets from cold vertical surface by ultrasonic vibration. *Experimental Thermal and Fluid Science* 53: 17–25.

Lowe MJS (1995) Matrix Techniques for Modeling Ultrasonic Waves in Multilayered Media. *IEEE Transactions on Ultrasonics, Ferroelectrics, and Frequency Control* 42(4): 525–542.

Menini R and Farzaneh M (2011) Advanced Icephobic Coatings. *Journal of Adhesion Science and Technology* 25(9): 971–992.

Młyniec A, Ambroziński Ł, Paćko P, Bednarz J, Staszewski W and Uhl T (2014) Adaptive de-icing system - numerical simulations and laboratory experimental validation. *International Journal of Applied Electromagnetics and Mechanics* 46(4): 997–1008.

Overmeyer A, Palacios JL, Smith EC and Royer R (2011) Rotating Testing of a Low-Power, Non-Thermal Ultrasonic De-icing System for Helicopter Rotor Blades. In: *SAE 2011 International Conference on Aircraft and Engine Icing and Ground Deicing, Chicago, Illinois*.

Palacios JL (2006) Ultrasonic Shear and Lamb Wave Interface Stress for Helicopter Rotor De-Icing Purposes. In: *47th AIAA Structural Dynamics & Materials, Newport, Rhode Island*.

Palacios JL (2008) *Design, Fabrication and Testing of an Ultrasonic De-icing System for Helicopter Blades*. PhD Thesis, Pennsylvania State University. Department of Aerospace Engineering.

Palacios JL and Smith EC (2008) Investigation of an Ultrasonic Ice Protection System for Helicopter Rotor Blades. In: *American Helicopter Society 64th Annual Forum, Montreal, Canada*.

Palacios JL, Smith EC, Rose JL and Royer R (2011a) Instantaneous De-Icing of Freezer Ice via Ultrasonic Actuation. *AIAA Journal* 49(6): 1158–1167.

Palacios JL, Smith EC, Rose JL and Royer R (2011b) Ultrasonic De-Icing of Wind-Tunnel Impact Icing. *Journal of Aircraft* 48(3): 1020–1027.

Ramanathan S (2005) *An Investigation on the Deicing of Helicopter Blades Using Shear Horizontal Guided Waves*. PhD Thesis, Pennsylvania State University. Department of Engineering Science and Mechanics.

Seppings RA (2005) *Investigation of Ice Removal From Cooled Metal Surfaces*. PhD Thesis, Imperial College, Mechanical Engineering Department, University of London.

Simonetti F (2004) Lamb wave propagation in elastic plates coated with viscoelastic materials. *The Journal of the Acoustical Society of America* 115(5): 2041–2053.

Tan H, Xu G, Tao T, Sun X and Yao W (2015) Experimental investigation on the defrosting performance of a finned-tube evaporator using intermittent ultrasonic vibration. *Applied Energy* 158: 220–232.

Vekinis G, Ashby MF and Beaumont PWR (1993) Plaster of paris as a model material for brittle porous solids. *Journal of Materials Science* 28(12): 3221–3227.

Voyiadjis GZ and Woelke, P (2008) *Elasto-Plastic and Damage Analysis of Plates and Shells*. Springer Berlin Heidelberg.

Wang Z, Xu Y and Gu Y (2015) A light lithium niobate transducer design and ultrasonic de-icing research for aircraft wing. *Energy* 87: 173–181.

Zhu Y (2010) *Structural Tailoring and Actuation Studies for Low Power Ultrasonic De-icing of Aluminium and Composite Plates*. PhD Thesis, Pennsylvania State University. Department of Engineering Science and Mechanics.